MATERIALS CHEMISTRY FRONTIERS

RESEARCH ARTICLE

View Article Online
View Journal | View Issue

Cite this: *Mater. Chem. Front.*, 2025, **9**, 1410

Highly stable electrofluorochromic switching of aggregation-induced emission-active conjugated polymers†

Ran Tao, ‡[a] Bryan Yat Kit Hui, ‡[ab] Kang Le Osmund Chin, [a] Xiang Yun Debbie Soo, [c] Danwei Zhang, [c] Syed Ali Abbas Abedi, [b] Pengqing Bi, [c] Xiaogang Liu, *[b] Jianwei Xu *[ad] and Ming Hui Chua *[a]

The development of aggregation-induced emission (AIE) luminogens for electrofluorochromic (EFC) applications has gained traction in recent years, yet challenges such as achieving stable and reversible fluorescence switching remain. In this study, we report a series of six conjugated polymers with AIE and aggregation-induced enhanced emission (AIEE) properties, synthesized from two novel tetraphenylethylene (TPE)-based monomers designed and functionalized with diphenylamine groups in distinct vicinal and geminal configurations. These polymers exhibit reversible electrochromic (EC) switching between yellow and purple colours, coupled with efficient EFC quenching of yellow and orange fluorescence upon application of positive voltage. EFC performance evaluations show impressive fluorescence turn-off/turn-on ($I_{OFF/ON}$) ratios of up to 37.3 and exceptional switching stability, maintaining functionality across 2500 cycles. Computational analyses suggest that both Förster resonance energy transfer (FRET) and electron transfer (ET) processes are critical to the observed fluorescence quenching. These findings not only provide valuable mechanistic insights but also open new pathways for the design of AIE-active materials with enhanced EFC performance and durability for targeted real-life applications.

Received 13th January 2025,
Accepted 17th March 2025

DOI: 10.1039/d5qm00035a

rsc.li/frontiers-materials

Introduction

Electrochromic (EC) and electrofluorochromic (EFC) materials exhibit reversible switching of colour and fluorescence, respectively, when an external voltage is applied. Such materials received significant attention as they demonstrate vast applications in smart windows, sensing, and optical displays.[1–4] While there has been tremendous progress and extensive research in developing EC materials, from inorganic oxides to metal complexes and conjugated polymers, EFC materials are relatively less studied. Yet their prominent applications in optoelectronic devices, optical displays, memory devices, and biological and chemical sensors highlighted their importance, necessitating further developments.[3,5–7] Amongst the various classes of reported EFC materials, including metal complexes, organic small molecules, and polymers,[4,8–10] fluorescent conjugated polymers offer the advantages of solution processability, lightweight, film flexibility, and tuneable optical properties *via* rational structural designs, thus making them ideal material candidates for EFC-related applications, particularly for the fabrication of flexible devices.

Many common luminogens tend to display an aggregation-caused quenching (ACQ) effect, limiting their applications in optoelectronics, including EFC applications. Thankfully, the discovery of aggregation-induced emission (AIE) phenomena in certain classes of luminogens has helped to overcome this thorny problem.[11] AIE luminogens are non-emissive in dilute solutions but become highly emissive when aggregated due to the restriction of intramolecular motions (RIM).[12,13] Likewise, the enhancement of a weakly emissive luminogen's emission intensity upon aggregation is referred to as aggregation-induced emission enhancement (AIEE). AIE and AIEE luminogens have since been widely exploited across various applications, ranging from chemosensing to optoelectronics and medical technology.[14–16]

[a] *Institute of Sustainability for Chemicals, Energy and Environment (ISCE²), Agency for Science, Technology and Research (A*STAR), Singapore. 1 Pesek Road, Jurong Island, 627833, Singapore. E-mail: chua_ming_hui@isce2.a-star.edu.sg, xu_jianwei@isce2.a-star.edu.sg*
[b] *Science, Math and Technology Cluster, Singapore University of Technology and Design (SUTD), 8 Somapah Road, Singapore, 487372, Singapore. E-mail: xiaogang_liu@sutd.edu.sg*
[c] *Institute of Materials Research and Engineering (IMRE), Agency for Science, Technology and Research (A*STAR), 2 Fusionopolis Way, Innovis, #08-03, Singapore, 138634, Singapore*
[d] *Department of Chemistry, National University of Singapore (NUS), Singapore. 3 Science Drive 3, 117543, Singapore*

† Electronic supplementary information (ESI) available. See DOI: https://doi.org/10.1039/d5qm00035a

‡ These authors contributed equally to this manuscript.

AIE-active moieties, such as tetraphenylethylene (TPE), hexaphenylsilole (HPS), and distyrylanthracene (DSA), have also become common scaffolds for constructing functional AIE materials.

EFC materials benefit from having AIE properties as it allows for intense fluorescence in assembled thin-film devices, which often translates to enhanced EFC switching properties, such as larger fluorescence contrast ratios, which is defined as the fluorescence intensity of the devices when an external voltage is turned-off *versus* when it is turned-on ($I_{OFF/ON}$).[17] To date, there has been a surge in several novel AIE-active EFC materials reported, comprising small molecules and polymers, including polyimides and polyacrylates, reflecting the growing interest in this area.[7,18–26] The delocalized π-electron system along the backbones of conjugated polymers enables efficient charge transport, making them excellent EC materials. Likewise, we believe that the same applies to EFC materials.

Reports of AIE-active EFC-conjugated polymers are, however, scarce. Xu's group earlier reported a 3,4-propylenedioxythiophene (ProDOT)–TPE copolymer that switches yellow-green fluorescence at ±2.5 V.[27] Niu and Wang *et al.* then studied the EFC properties of a novel 4,4′-bis[*N*-(1-naphthyl)-*N*-phenylamino]biphenyl–TPE copolymer, whose blue fluorescence was quenched at an applied voltage of +1.6 V.[28] Qin and Tang *et al.* later synthesized two novel polymers in which the electroactive triphenylamine (TPA) was co-polymerized respectively with TPE and dithienyldiphenylethylene co-monomers.[28] These two TPA-containing green and orange emissive polymers, which were stable for up to 50 cycles of EFC switching, were subsequently used to fabricate information storage and anti-counterfeiting devices. More recently, Zhang's group prepared two homopolymers bearing triphenylacrylonitrile and diphenylacrylonitrile-functionalized TPA monomers exhibiting ultra-fast EFC switching of yellow fluorescence.[29] While these polymers generally demonstrate desirable EFC switching properties, with some achieving high $I_{OFF/ON}$ and ultrafast response times, most EFC reported devices exhibit switching stabilities of up to only 100 cycles. As such, it is imperative to improve on the long-term switching stability of EFC devices through materials development, which is crucial for practical applications. Additionally, the lack of computational studies related to the EFC mechanistic pathways limits the rational design of new AIE-EFC materials, which is an area where more could be done.[30]

We herein report six novel conjugated polymers based on two new TPA-functionalized TPE monomers (Scheme 1). Unlike many reported polymers in which the electroactive TPA is part of the conjugated polymer backbones, diphenylamine (DPA) moieties were functionalized onto TPE monomers in geminal and vicinal configurations. The two regioisomeric monomers, v-DPATPE and g-DPATPE, were then co-polymerized with

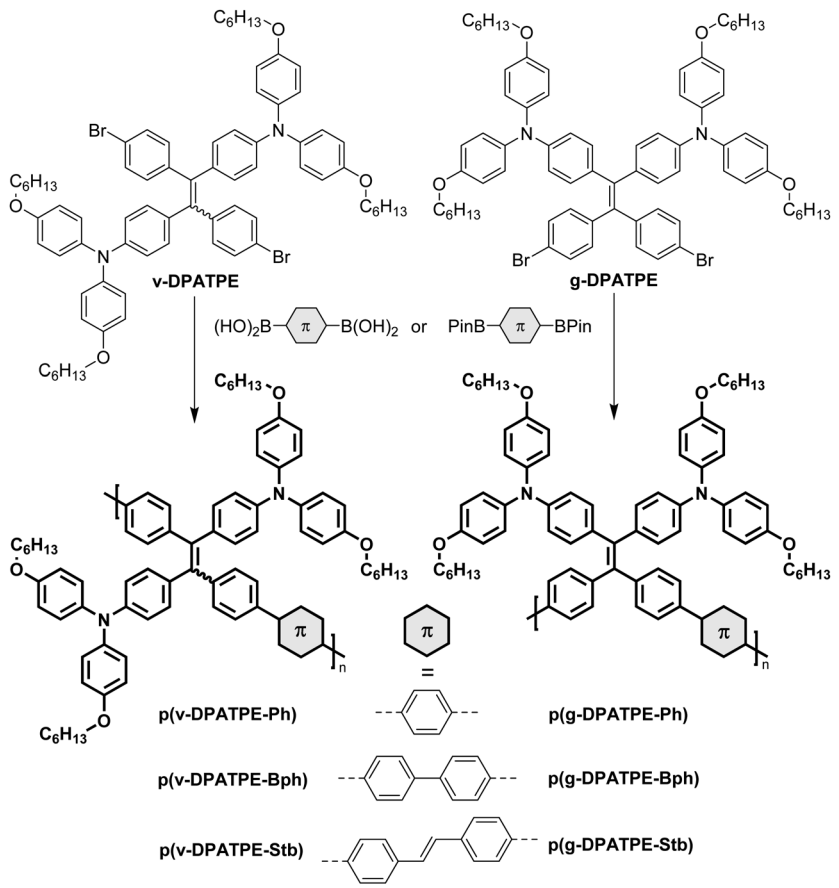

Scheme 1 Chemical structures of novel monomers v-DPATPE and g-DPATPE, and AIE-active EFC conjugated polymers, p(v-DPATPE-Ph), p(g-DPATPE-Ph), p(v-DPATPE-Bph), p(g-DPATPE-Bph), p(v-DPATPE-Stb), and p(g-DPATPE-Stb).

phenyl, biphenyl, and stilbene co-monomers to afford polymers p(v-DPATPE-Ph), p(g-DPATPE-Ph), p(v-DPATPE-Bph), p(g-DPATPE-Bph), p(v-DPATPE-Stb), and p(g-DPATPE-Stb). The six polymers were found to exhibit bright yellow to orange fluorescence in thin film EFC devices owing to their AIE and AIEE properties, which were effectively quenched upon the application of relatively low voltages of +1.3 to +1.5 V. The polymers exhibited excellent EFC switching performance, with $I_{OFF/ON}$ ratios and long-term stability of up to 37.3 and 2500 cycles, respectively. Our computational studies further suggested a possible Förster resonance energy transfer (FRET), as well as electron transfer (ET), as plausible mechanisms for the efficient EFC fluorescence quenching for this series of polymers. These findings can therefore provide insights to guide future rational designs of high-performance AIE-active EFC conjugated polymers.

Results and discussion

Polymer synthesis and characterization

Two novel monomers, g-DPATPE and v-DPATPE, were designed by decorating the TPE unit with two diphenylamine moieties in the geminal and vicinal fashions, respectively. The TPE scaffold was selected to confer AIE properties, whereas the resultant TPA portions provide the necessary redox activity for EC and EFC applications. Meanwhile, hexyloxyl chains were introduced to improve the polymer solubility. Monomer g-DPATPE was synthesized through McMurry coupling between 4,4′-dibromobenzophenone and intermediate **1**, which was prepared *via* Buchwald–Hartwig amination of 4,4′-dibromobenzophenone with bis(4-(hexyloxy)phenyl)amine, whereas monomer v-DPATPE was obtained *via* McMurry coupling of intermediate **2**, synthesized *via* nucleophilic aromatic substitution of 4-bromo-4′-fluorobenzophenone with bis(4-(hexyloxy)phenyl)amine (Scheme S1, ESI†). The presence of both AIE and redox-active components in a single monomer allows for versatility in polymerizing with other co-monomers, potentially affording AIE-active EFC conjugated polymers with tuneable opto-electrochemical properties.

Herein, both monomers were polymerized with the diboronic acids and esters of three different π-linkers, phenyl, biphenyl, and (*E*)-stilbene (denoted Ph, Bph, and Stb), *via* Suzuki cross-coupling, catalysed by $Pd_2(dba)_3$ in the presence of SPhos, to afford six polymers p(v-DPATPE-Ph), p(g-DPATPE-Ph), p(v-DPATPE-Bph), p(g-DPATPE-Bph), p(v-DPATPE-Stb), and p(g-DPATPE-Stb) (Scheme 1). Comparing the different π-linkers, polymers with biphenyl co-monomers were obtained with the best yields whereas polymers with stilbene co-monomers generally have higher molecular weights than their counterparts (Table 1). We believe that the extent of steric hindrance faced between monomers during the polymerization reaction can affect the degree of polymerization and molecular weight. Both v-DPATPE and g-DPATPE monomers are inherently sterically congested and co-polymerizing with diboronic acids of Ph, which is laterally the shortest π-linker amongst the three, therefore, experienced the largest steric hindrance during polymerization, which accounts for the relatively smaller molecular weights for p(v-DPATPE-Ph) and p(g-DPATPE-Ph) compared to polymers containing Bph and Stb π-linkers. On the other hand, the greater structural flexibility in stilbene's C=C bonds may have also enhanced polymer solubility, leading to larger molecular weights. Meanwhile, we observed that the vicinal series of polymers generally have larger PDIs presumably due to the presence of both *E* and *Z* isomers in v-DPATPE, whereby variations in polymer chain lengths arise from the different extent of steric hindrance imposed by the two isomers with co-monomers during polymerization. All six polymers exhibited excellent thermal stability with decomposition temperature (T_d) above 430 °C, as reflected by thermogravimetric analysis (Table 1).

Table 1 Mass and thermal properties of polymer series p(g-DPATPE) and p(v-DPATPE)

Polymer	Yield (%)	M_w[a] (kDa)	M_n[b] (kDa)	PDI[c]	T_d (in N_2)[d]
p(g-DPATPE-Ph)	62	15.5	8.5	1.82	442
p(g-DPATPE-Bph)	98	15.7	9.5	1.66	437
p(g-DPATPE-Stb)	72	16.5	11.0	1.50	433
p(v-DPATPE-Ph)	33	11.7	7.8	1.50	439
p(v-DPATPE-Bph)	99	43.6	20.0	2.18	435
p(v-DPATPE-Stb)	81	75.4	27.9	2.71	442

[a] Mass average molar mass. [b] Umber average molar mass. [c] Polydispersity index. [d] Decomposition temperature.

Optical and electrochemical properties

The UV-vis absorption spectra of the six polymers were measured in chloroform solutions (Fig. 1a and Table 2). The polymers exhibit maximum absorption (λ_{abs}^{soln}) ranging from 308 to 366 nm, with a general red-shifting trend as the π-linker increases in conjugation, going from phenyl to biphenyl to stilbene. Meanwhile, the vicinal polymers exhibit slightly more red-shifted λ_{abs}^{soln} compared to their geminal counterparts, reflecting the more effective electronic-conjugation achieved by the monomer-connection across the *E*-stilbene component of TPE. The six polymers generally possess high molar extinction coefficients (ε) ranging from 54 280 to 87 811 M^{-1} cm^{-1}. Polymers bearing phenyl and biphenyl π-linkers were observed to red-shift in absorption profiles and hence λ_{abs}^{film} when transitioning from solution to thin film states (Table 2 and Fig. S1, ESI†). Phenyl-containing polymers exhibited greater red-shifts than biphenyl ones with p(g-DPATPE-Ph) experiencing the greatest red-shift of 61 nm. In contrast, no change in λ_{abs}^{film} was observed for p(v-DPATPE-Stb). One plausible reason is that as the π-linker lengthens from phenyl to biphenyl and then to stilbene, the extent of conformational distortion in solutions between adjacent monomers along the polymer chain decreases relative to that in thin films which often adopts a more planar and extended conformation with lower energy. Additionally, the polymers may experience π–π interactions and aggregation effects in thin films, leading to lower energy and red-shifted λ_{abs}.

The optical bandgaps (E_g) of the six polymers derived from the onset absorption wavelength (λ_{onset}) were relatively consistent in the range of from 2.54 eV to 2.62 eV (Table 2). Polymers containing a stilbene π-linker exhibit slightly lower E_g compared

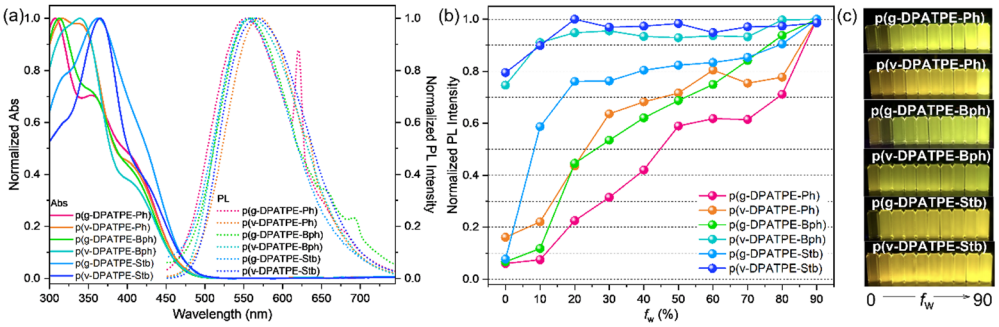

Fig. 1 (a) Normalized absorption (Abs) and photoluminescence (PL) spectra of p(g-DPATPE-Ph), p(v-DPATPE-Ph), p(g-DPATPE-Bph), p(v-DPATPE-Bph), p(g-DPATPE-Stb), and p(v-DPATPE-Stb) in chloroform solutions. (b) Plots of normalized PL intensity at respective emission maximum wavelengths (λ_{em}) *versus* the fraction of water (f_w) in water/THF solutions for the six polymers. (c) Photos showing fluorescence changes of the six polymers in 10 μM THF/water solutions of different f_w values (0–90%), irradiated at 365 nm.

Table 2 Summary of optical and electrochemical properties of polymers p(g-DPATPE-Ph), p(v-DPATPE-Ph), p(g-DPATPE-Bph), p(v-DPATPE-Bph), p(g-DPATPE-Stb), and p(v-DPATPE-Stb)

	Optical properties									Electrochemical properties				
Polymer	ε^a (M^{-1} cm^{-1})	$\lambda_{abs}^{soln b}$ (nm)	$\lambda_{onset}^{soln\ c}$ (nm)	$\lambda_{em}^{soln d}$ (nm)	$\Phi^{soln e}$ (%)	$\lambda_{abs}^{film b}$ (nm)	$\lambda_{onset}^{film\ c}$ (nm)	$\lambda_{em}^{film d}$ (nm)	$\Phi^{film f}$ (%)	$E_{ox}^{\ g}$ (eV)	$E_{HOMO}^{\ h}$ (eV)	$E_{LUMO}^{\ i}$ (eV)	$E_g^{soln j}$ (eV)	$E_g^{film j}$ (eV)
p(g-DPATPE-Ph)	60 687	308	474	545	0.95	369	484	543	28.75	0.21	−5.01	−2.40	2.62	2.56
p(v-DPATPE-Ph)	54 280	315	474	556	3.62	361	480	552	23.00	0.24	−5.04	−2.43	2.62	2.58
p(g-DPATPE-Bph)	80 434	312	476	548	0.54	333	482	546	25.51	0.30	−5.10	−2.50	2.61	2.57
p(v-DPATPE-Bph)	72 363	339	479	553	14.60	346	482	559	17.68	0.22	−5.02	−2.44	2.59	2.57
p(g-DPATPE-Stb)	68 496	360	486	556	0.77	361	515	553	9.39	0.36	−5.16	−2.60	2.55	2.41
p(v-DPATPE-Stb)	87 811	366	489	567	14.19	366	514	560	13.04	0.19	−4.99	−2.45	2.54	2.41

[a] Molar extinction coefficient. [b] Maximum absorption wavelength. [c] Onset absorption wavelength. [d] Emission maximum wavelength. [e] Fluorescence quantum yield in THF calculated with excitation at λ_{abs}^{soln} in reference to quinine sulphate in 0.5 M H_2SO_4, (F = 0.54), [C] = 1 × 10^{-5} M. [f] FL quantum yield of the polymer film spin-coated on ITO glass, measured at an excitation wavelength of 405 nm. [g] Onset oxidation potential measured by CV. [h] Calculated by the equation $E_{HOMO} = -(E_{ox} + 4.70)$.[31,32] [i] Calculated by the equation $E_{LUMO} = E_{HOMO} + E_g^{soln}$. [j] Optical bandgap, calculated from λ_{onset} through the equation $E_g = 1240/\lambda_{onset}$.

to those with biphenyl and phenyl π-linkers due to more extended conjugation. However, no significant differences in E_g were observed between vicinal and geminal polymers containing the same π-linkers. The oxidation onset potentials (E_{ox}) for the six polymers were obtained from the cyclic voltammetry (CV) measurements (Fig. S2–S7, ESI†), and the E_{HOMO} and E_{LUMO} values were subsequently calculated from the E_{ox} and E_g^{soln} values (Table 2). The E_{HOMO} and E_{LUMO} values are likewise fairly consistent across the six polymers (−4.99 to −5.16 eV, and −2.60 to −2.40 eV, respectively). Their relatively high E_{HOMO} values reflect the electron-rich nature of the six polymers due to the presence of TPA and TPE groups. Overall, the six polymers are rather electrochemically similar despite their slight variations in chemical structures.

The fluorescence properties of the six polymers were investigated in both solution (Fig. 1a) and thin-film states (Fig. S1, ESI†) (Table 2). All six polymers were observed to emit weak to moderate yellow fluorescence in chloroform solutions, characterized by single-banded photoluminescence spectra with maximum wavelengths (λ_{em}^{soln}) ranging from 545 to 567 nm. Comparatively longer λ_{em} were achieved with stilbene π-linkers and v-DPATPE monomers, relative to other π-linkers and g-DPATPE, respectively. It is noted that polymers containing v-DPATPE monomers exhibit larger solution fluorescence quantum yield compared to their counterparts bearing g-DPATPE monomers probably due to better π-conjugation across the vicinal series of polymers. Amongst the polymers, p(v-DPATPE-Bph) and p(v-DPATPE-Stb) exhibited the brightest emissions in solutions with fluorescence quantum yield (Φ^{soln}) of ∼14% (*vs.* 0.54–3.62% for the other polymers), which might be attributed to a combination of factors, including a more effective and extended π-conjugation across Bph and Stb (*vs.* Ph) π-linkers, the two polymers having relatively large molar absorptivity, and possible restriction of intramolecular motion and conformational locking caused by intramolecular folding and interchain interactions. The photoluminescence spectra and maximum wavelengths (λ_{em}^{film}) of the polymers in thin films were similarly red-shifted compared to their dilute solutions (Fig. S1, ESI,† Table 2). The thin films emitted bright yellow to orange fluorescence with λ_{em}^{film} of 543 to 560 nm and fluorescence quantum yields (Φ^{film}) ranging from 9.39 to 28.75%. The significant enhancement in Φ relative to solution states is attributed to AIE and AIEE properties of the polymers.

To investigate the AIE/AIEE properties of the six polymers, fluorescence changes of each polymer were studied at 10 μM in a THF/water binary solvent mixture with varying proportions (Fig. S8, ESI†). Aggregation arising from increasing the

proportion of water anti-solvent relative to THF good solvent led to significant enhancement in the fluorescence intensities for p(g-DPATPE-Ph), p(v-DPATPE-Ph), p(g-DPATPE-Bph), and p(g-DPATPE-Stb), with Φ^{soln} increasing from 0.95, 3.62, 0.54, and 0.77% at fraction of water (f_w) of 0 to 14.06, 22.38, 6.92, and 9.25% at f_w = 90%, respectively. This reflects their AIE properties. In contrast, smaller enhancements in fluorescence were observed going from f_w = 0 to 90% for initially moderately fluorescent p(v-DPATPE-Bph) and p(v-DPATPE-Stb) with Φ^{soln} increasing from 14.60 and 14.19% to 22.93 and 19.52%, respectively, as f_w increased from f_w = 0 to 90%, indicating their AIEE characteristics (Fig. 1b and c). The AIE and AIEE properties were mainly attributed to the rotor-like structures of TPA and TPE components on the DPATPE monomers, and additionally, the stilbene π-linker for p(g-DPATPE-Stb) and p(v-DPATPE-Stb), instilling RIM upon aggregation.

Electrochromic properties studies

EC devices (ECDs) were fabricated using the six polymers to study their EC and EFC properties. With the exception of p(v-DPATPE-Ph), the remaining five polymers were visually found to possess excellent film-forming properties. Scanning electron microscopy (SEM) under 1500× and 6000× magnifications shows that the spin-coated polymer films on ITO-glass substrates generally possess homogenous morphologies without any observable formation of particulates with only minor streaks noted in the films of p(v-DPATPE-Ph) (Fig. S9–S14, ESI†). These uniform morphologies are believed to contribute to the overall favourable ECD switching performances across all six polymers.

Spectroelectrochemistry studies were performed by applying incremental voltages to the ECDs. While the six polymers show no colour or spectral changes under negative voltages up to −2.4 V (Fig. S15, ESI†), gradual spectral changes in the visible to near-infrared (NIR) region were observed upon increasing positive voltage, saturating at *ca.* +1.5 to +1.7 V. The polymers change from yellow to various shades of purple colour in the oxidised states (Fig. 2). The six neutral polymers show only one absorption band in the UV region (λ_{abs}^{film} at *ca.* 333 to 369 nm) corresponding to the locally excited π–π* transition from the DPA fragment to the TPE unit (Fig. S22, ESI†). As the applied voltages increase, new absorption bands in the visible and NIR regions emerge due to the electro-oxidation of the polymers, resulting in the formation of cationic polarons and bipolarons. Interestingly, electro-oxidation of the geminal polymer series reveals a distinct absorption band at *ca.* 745 nm, accompanied by lower intensity broad absorption bands at *ca.* 535 nm and from *ca.* 850 to 1400 nm. Meanwhile, the vicinal polymers series reveal a broader new absorption band over *ca.* 400 to 1000 nm, with one peak for p(v-DPATPE-Ph) and two defined peaks for p(v-DPATPE-Bph) and p(v-DPATPE-Stb), respectively.

Colorimetric analysis was performed to determine the colour coordinates of the six polymers in the neutral and oxidised states according to the CIE 1976 *L*a*b** colour space (Table S1 and Fig. S16, ESI†). The yellow-to-purple colour changes were characterized by a general trend of a stark shift in *a** from negative (green) to positive (red) and a decrease in *b** from positive (yellow) to the negative (blue) region, accompanied by a decrease in *L** values, indicating a drop in perceptual lightness in oxidised colour. Overall, based on the colorimetric analysis,

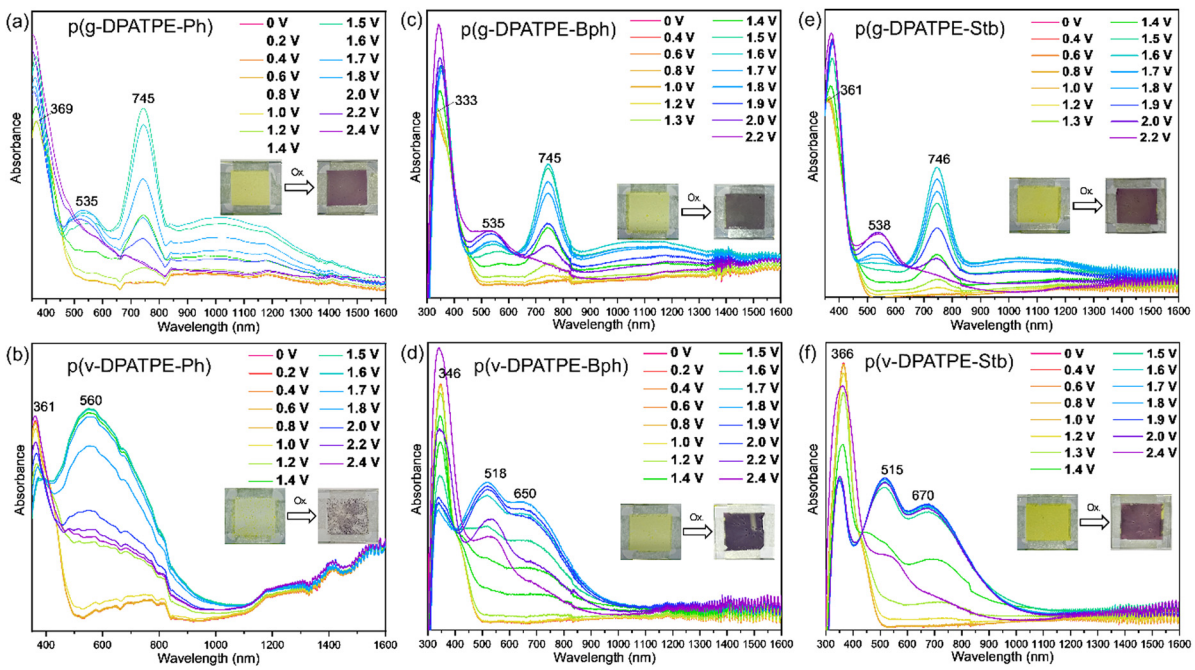

Fig. 2 EC Spectroelectrochemistry of (a) p(g-DPATPE-Ph), (b) p(v-DPATPE-Ph), (c) p(g-DPATPE-Bph), (d) p(v-DPATPE-Bph), (e) p(g-DPATPE-Stb), and (f) p(v-DPATPE-Stb) measured in thin film ECDs fabricated with increasing applied positive voltages. Insets are photos showing the colour changes of the ECDs.

the polymers with stilbene π-linker reveal the drastic change in colour as reflected by the relatively larger magnitude of change in L^*, a^*, and b^* values.

Square wave potential step chronoabsorptometry studies were subsequently performed to assess the EC switching properties of the six polymers at their respective newly emerged bands (Fig. S17, ESI†). A general trend was observed where optical contrasts (OC) increase with lengthening of π-linker from phenyl to biphenyl to stilbene. The vicinal polymers series also generally exhibit larger OCs than their geminal counterparts. These reflect the correlation between OC and the extent of π-conjugation in the polymers. When switching the applied voltage at ±2.0 V with time interval (Δt) of 40 s, p(g-DPATPE-Stb) was found to exhibit the best OC (at 746 nm) among the six polymers, reaching 70.1%. Although a slight reduction in average OCs was observed as Δt decreased from 40 to 30, 20, and 10 s, the cycling (transmittance *vs.* time) waveforms remained relatively stable with no signs of performance degradation.

Electrofluorochromic property studies

EFC spectroelectrochemistry studies were performed for the six polymers using the fabricated ECDs. All six polymers emit bright yellow to orange fluorescence in their neutral states, which are progressively quenched when an external voltage is incrementally applied from 0 to +1.5 V (Fig. 3). Considerable fluorescence quenching occurs at *ca.* +0.8 V, and the polymers' fluorescence is completely quenched at +1.3 to +1.5 V. This is smaller in magnitude compared to the applied voltage required for the complete first oxidation (+1.5 to +1.7 V) in EC spectroelectrochemistry, suggesting that the EFC process (and fluorescence quenching) occurs upon partial oxidation. The Φ^{film} of the six polymers, upon undergoing electro-oxidation, were all found to be zero.

Square wave potential step chronofluorometry studies were performed to evaluate the EFC switching properties of the six polymers at their respective λ_{em}^{film} (Fig. S18, ESI†). During these studies, the fluorescence intensities of ECDs were monitored over time as applied voltages were repeatedly switched between positive and negative voltages of the same amplitude at different Δt. One parameter used to determine the contrast in fluorescence switching is $I_{OFF/ON}$, which is the ratio of the fluorescence intensity of the ECD when the external voltage that causes fluorescence quenching is discontinued (I_{OFF}), relative to the ECD's fluorescence intensity when that external voltage is supplied (I_{ON}). Our studies show that p(g-DPATPE-Ph) has the largest contrast amongst the six polymers, with a high $I_{OFF/ON}$ of 37.3 switching at ±1.5 V with Δt = 40 s (Fig. 4a). This value is notably higher than that of p(g-DPATPE-Bph), which shows the second largest fluorescence contrast, registering an $I_{OFF/ON}$ of 25.8 at the same Δt (Fig. S18, ESI†).

Meanwhile, reducing Δt for the switching studies reasonably led to a decrease in contrast as there was less time available to oxidise the polymers, and subsequently reduce them back to the neutral state. Unlike polymers p(g-DPATPE-Bph), p(g-DPATPE-Stb), and p(v-DPATPE-Stb) which experience considerable drop in contrasts as switching Δt decreases due to both a decrease in I_{OFF} and an increase in I_{ON}, the drop in contrast for p(g-DPATPE-Ph) remained relatively modest as the intensity differences between I_{OFF} and I_{ON} at Δt = 20, 10, and 5 s are only

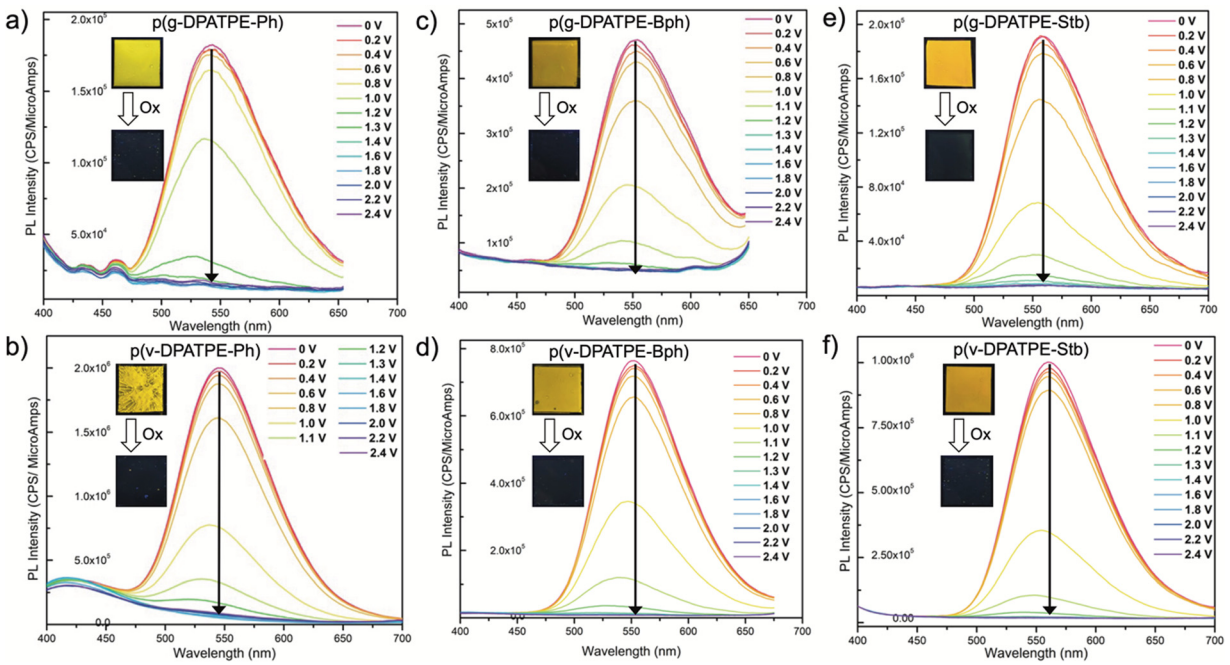

Fig. 3 EFC spectroelectrochemistry of (a) p(g-DPATPE-Ph), (b) p(v-DPATPE-Ph), (c) p(g-DPATPE-Bph), (d) p(v-DPATPE-Bph), (e) p(g-DPATPE-Stb), and (f) p(v-DPATPE-Stb) measured in thin film ECDs fabricated with increasing applied positive voltages. Insets are photos showing the fluorescence changes of the ECDs, irradiated at 365 nm.

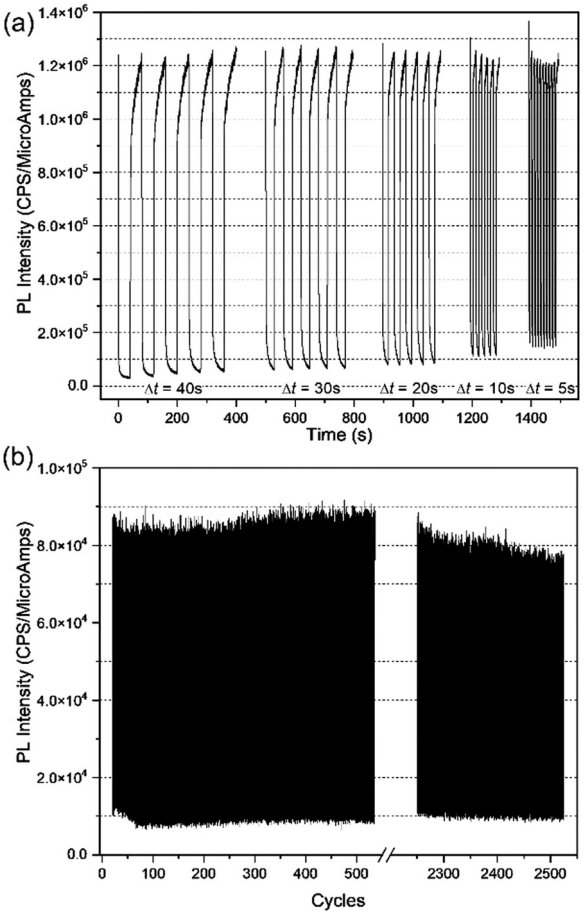

Fig. 4 (a) EFC chronofluorometry of p(g-DPATPE-Ph) ECD, switching at ±1.5 V at different Δ*t* of 40, 30, 20, 10, and 5 s. (b) Long-term EFC switching stability of p(g-DPATPE-Ph) ECD, with voltage alternating at ±1.5 V at Δ*t* of 20 s, for 2500 cycles.

ca. 3, 6, and 11% less, respectively, than those at Δ*t* = 40 s, with no obvious contrast change observed for Δ*t* = 30 s (Fig. 4a). We noted that for p(g-DPATPE-Ph), I_{ON} remained relatively constant even as Δ*t* was reduced, while I_{OFF} was slightly increased.

The polymers' EFC switching contrasts at different Δ*t* are related not only to the Φ^{film} in ECDs, but also to the switching response times, which are defined as the time taken to achieve 95% of maximum fluorescence quenching (τ_{OFF}) and the time taken to restore 95% of initial fluorescence (τ_{ON}) through the application of positive and negative voltages, respectively (Fig. S19 and S20, ESI†). Ideally, EFC polymers should have shorter τ_{OFF} and τ_{ON} to achieve full or maximum fluorescence contrasts at shorter switching Δ*t*. The six polymers possess τ_{OFF} ranging from 5.5 to 40.6 s, with p(g-DPATPE-Stb) exhibiting the shortest response time, and p(v-DPATPE-Ph) the longest. In contrast, the polymers' τ_{ON} values range between 11.1 and 57.6 s, with p(g-DPATPE-Ph) and p(v-DPATPE-Ph) being the shortest and longest, respectively. Overall, p(g-DPATPE-Stb) demonstrates the best EFC switching response times with τ_{OFF} and τ_{ON} of 5.5 and 11.4 s, respectively. We also observed a general trend where the geminal series of polymers exhibit shorter response times than their vicinal counterparts (Table S2, ESI†).

The long-term EFC switching stability was further studied for polymers with phenyl π-linker, p(g-DPATPE-Ph) and p(v-DPATPE-Ph), by alternating applied voltages of ±1.5 V at Δ*t* of 20 s (Fig. 4b and Fig. S21, ESI†). Both polymers showed remarkable switching stability for at least 500 cycles with no observable decrease in fluorescence contrasts. To the best of our knowledge, this result is amongst the best EFC switching stability reported for most known AIE EFC polymers (Table S4, ESI†). The switching stability study of p(g-DPATPE-Ph) was further extended to 2500 cycles, where only a modest drop in fluorescence contrast of *ca.* 10% was recorded (Fig. 4b), which we believe constitutes the best stability results reported to date. The relatively desirable EFC switching performance of this series of polymers also likely stems from the fact that conjugated polymers typically have better electronic communication compared to non-conjugated ones, which are the cases for a large number of reported AIE-active EFC polymers (Scheme S2 and Table S5, ESI†). Overall, considering Φ^{film}, fluorescence switching contrasts, response times, and most importantly, long-term stability, we believe p(g-DPATPE-Ph) may be considered the best performing polymer amongst the six novel polymers for EFC switching.

Computational and mechanistic studies

From the structure–property relationship studies above, we observed that the polymers do not exhibit the mirroring trends in EC and EFC switching performance relative to their structures. For instance, p(g-DPATPE-Ph) exhibits modest OC for EC switching but superior fluorescence contrast for EFC switching.

To better understand the mechanisms driving the EFC properties of the six polymers, density functional theory (DFT) and time-dependent DFT (TD-DFT) calculations were performed using the Gaussian 16A program.[33–35] Geometry optimization was carried out on representative units of each polymer, consisting of one repeating unit with hexyloxyl chains replaced with methoxy groups, using the ωB97XD functional[36] and the def2SVP basis set[37] in a vacuum. Ground state geometry optimisation revealed that the representative units adopt highly puckered geometries, regardless of the functionalization positions of the two DPA groups and the π-linker groups on the bulky TPE unit, due to steric hindrance (Fig. S22, ESI†). The common dihedral angles ϕ_{1-5} between DPA, TPE, and their π-linker groups range from 23.9 to 67.1° (Table S3, ESI†), suggesting that neither series exhibits extended conjugation throughout the polymers. To further investigate the EFC quenching mechanism, phenyl-containing polymers p(g-DPATPE-Ph) and p(v-DPATPE-Ph) were selected as model systems.

We propose that fluorescence quenching occurs *via* two concurrent mechanisms. The first mechanism is Förster resonance energy transfer (FRET) between an excited state neutral unit and a ground state cationic radical unit (generated upon electro-oxidation) (Fig. 5a). The initial photoexcitation of a neutral unit from the singlet ground state (S_0) to the first singlet excited state (S_1) corresponds to an ICT process from the DPA fragments (hole) to the TPE and π-linker regions (electron). Subsequent relaxation from S_1 back to S_0 of the

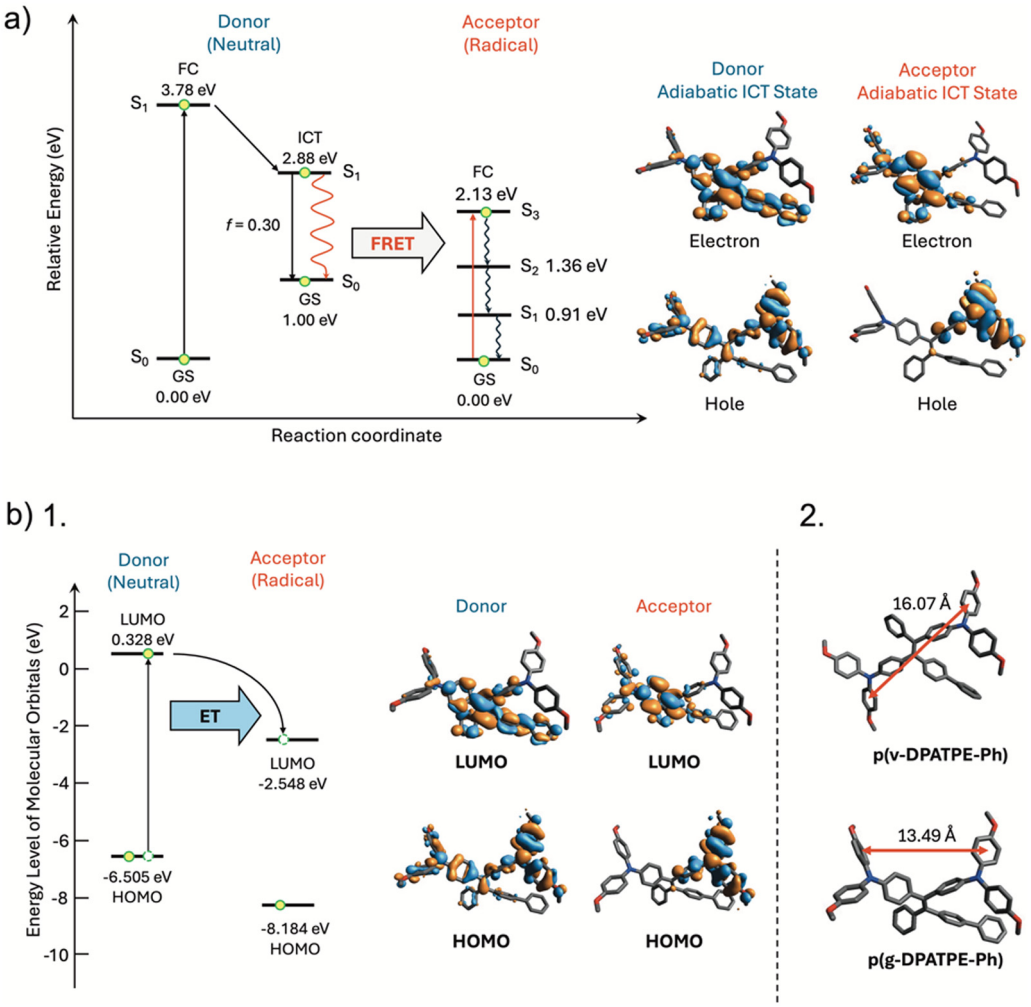

Fig. 5 (a) Schematic illustration of the potential energy surfaces of a neutral and radical representative unit of p(g-DPATPE-Ph) and the proposed FRET mechanism with calculated excitation/de-excitation energy (as well as oscillator strength *f*); for the radical unit, only the vertical excitation process is shown. (b) 1. Schematic illustration of the molecular orbitals of a neutral and radical representative p(g-DPATPE-Ph) unit of and the proposed ET mechanism; 2. Measured distance between two DPA fragments in the vicinal and geminal isomers to highlight differences in ET efficiency. (GS: ground state; FC: Frank–Condon state; ICT: intramolecular charge transfer state; IC: internal conversion; CI: conical intersection; HOMO: highest occupied molecular orbital; LUMO: lowest unoccupied molecular orbital).

excited neutral unit was modelled to be a radiative emission of 1.88 eV with an oscillator strength of $f = 0.30$, which agrees with the fluorescence observed in the AIEE studies. On the other hand, the state model predicts that the radical unit can be vertically excited from S_0 to S_2–S_3, with an energy gap of 1.36–2.13 eV. As this energy gap of the radical unit closely overlaps with the S_1–S_0 emission energy gap of the excited donor (1.88 eV), we predict that FRET would occur between an excited neutral unit and a ground state radical unit. Following FRET, internal conversion (IC) occurs from S_2/S_3 to S_1 in the excited state radical unit, as per Kasha's rule. Upon further geometry optimization of the radical unit in the S_1 state, our calculations indicate the occurrence of a conical intersection (CI) between the two potential energy surfaces (S_1 and S_0),[38] which facilitates rapid non-radiative decay to the ground state. As observed from EFC and EC studies where the neutral polymers' emission bands in the 500–700 nm region (Fig. S1, ESI†) overlap with the newly generated absorption bands of the cationic radical quenchers (Fig. 2), this spectral overlap strongly corroborates FRET between proximal neutral polymers and cationic radical quenchers. Moreover, the rapid decay in the radical quencher could quench the fluorescence of many surrounding neutral fluorophores, thus boosting the fluorescence turn-on ratio in comparison to OC changes.

The second proposed mechanism involves an electron transfer (ET) between two neighbouring DPA units in the monomer. The molecular orbital (MO) diagram (Fig. 5b1) depicts that the LUMO of the radical unit is more stable than the LUMO of the neutral unit, which potentially allows for ET between the two LUMOs upon photoexcitation of an electron from the HOMO to the LUMO in the neutral unit. The rapid decay of electron-transfer states allows a single radical to quench multiple nearby neutral molecules. This mechanism significantly enhances the sensitivity of the fluorescence response compared to the visual colour changes.

The observed differences in EFC properties among the polymers can be attributed to variations in π-linker groups, intermolecular packing, and stereoisomerism. These factors critically affect the distances between both energy donors and acceptors, as well as electron donors and acceptors, thereby impacting quenching efficiency.[39] For example, in our calculations, the distance between the DPA units is 13.49 Å in the representative unit of p(g-DPATPE-Ph) compared to 16.07 Å in p(v-DPATPE-Ph) (Fig. 5b2). Thus, the geminal series of polymers is expected to have more efficient energy and electron transfer, leading to effective fluorescence quenching, higher I_{OFF}/I_{ON} ratios and reduced response times relative to the vicinal isomers.

Conclusions

In summary, we have designed two novel monomers, g-DPATPE and v-DPATPE, incorporating both the AIE-active TPE and electroactive TPA components in each single monomer. The two monomers were subsequently co-polymerized with three different π-linkers monomers (phenyl, biphenyl and *E*-stilbene) to afford six novel AIE/AIEE conjugated polymers, p(g-DPATPE-Ph), p(v-DPATPE-Ph), p(g-DPATPE-Bph), p(v-DPATPE-Bph), p(g-DPATPE-Stb), and p(v-DPATPE-Stb). The EC and EFC properties of the six polymers were studied using assembled thin film ECDs, in which the application of positive voltages induced electro-oxidation, lead to a reversible colour change from yellow to purple, alongside the quenching of bright yellow to orange fluorescence, respectively.

The six polymers exhibited promising EC and EFC switching contrasts, with p(g-DPATPE-Stb) achieving the highest OC of 70.1% for EC switching at 746 nm, whereas p(g-DPATPE-Ph) demonstrated the highest $I_{OFF/ON}$ of 37.3 for EFC switching at 543 nm. In addition, p(g-DPATPE-Ph) and p(v-DPATPE-Ph) exhibited excellent long-term EFC switching stability of at least 500 cycles without significant contrast degradation, and notably, the latter remained relatively stable up to 2500 switching cycles with only a *ca.* 10% drop in performance. To the best of our knowledge, these results represent the best long-term switching stability reported for AIE EFC materials to date. DFT and TD-DFT calculations were further performed to gain greater mechanistic insights into the EFC fluorescence quenching process of the polymers, where FRET with CI, and ET were proposed to reasonably explain the observed trends in EFC properties.

Thus, we have demonstrated the potential of the two novel monomers, g-DPATPE and v-DPATPE, to construct high-performance EC and AIE/AIEE-active EFC materials, as they can be coupled in a versatile manner with other co-monomers to further tune the colour, fluorescence, and EC/EFC properties. More importantly, the experimental and computational findings from this study provided crucial insights into structure–property relationships and mechanisms that can guide future designs of high-performance AIE-active EFC conjugated polymeric materials, particularly possessing robust fluorescence switching stability, which remain limited in examples but show significant promise.

Author contributions

R. Tao contributed to investigation work involving synthesizing and characterization of polymers, as well as visualization, writing the original draft, review, and editing of the manuscript. B. Y. K. Hui likewise contributed to investigation work involving polymer synthesis, device fabrication and testing, and computational studies, in addition to visualization, writing the original draft, review, and editing of the manuscript. K. L. O. Chin contributed to investigation work involving the characterization of polymers, device fabrication, and testing. X. Y. D. Soo, D. Zhang, and P. Bi supported various characterization studies for the polymers synthesized (investigation). S. A. A. Abedi aided in the methodology for computational studies. X. Liu and J. Xu provided supervision, funding acquisition, and review and editing of the manuscript. M. H. Chua conceptualized this work, and provided supervision, project administration, and funding acquisition. He was also involved in the visualization and writing (review and editing) of the manuscript.

Data availability

All experimental details and data supporting the findings of this article are available within the paper and also included in the ESI.†

Conflicts of interest

The authors have no conflict to declare.

Acknowledgements

The authors would like to acknowledge funding support from the Agency for Science, Technology and Research, Singapore (A*STAR) 2020 Career Development Fund (grant number: C210112042), the A*STAR HTCO Fund (grant number: C231218001), and the Singapore University of Technology and Design (SUTD) Kickstarter Initiative (grant number: SKI 2021_03_10). The authors are also grateful for the computing service of SUTD and the National Supercomputing Centre (Singapore).

References

1 M. H. Chua, Q. Zhu, K. W. Shah and J. Xu, Electroluminochromic Materials: From Molecules to Polymers, *Polymers*, 2019, **11**, 98.
2 S. Kandpal, T. Ghosh, C. Rani, A. Chaudhary, J. Park, P. S. Lee and R. Kumar, Multifunctional Electrochromic Devices for Energy Applications, *ACS Energy Lett.*, 2023, **8**, 1870–1886.
3 G. A. Corrente and A. Beneduci, Overview on the Recent Progress on Electrofluorochromic Materials and Devices: A Critical Synopsis, *Adv. Opt. Mater.*, 2020, **8**, 2000887.
4 I. Seddiki, B. I. N'Diaye and W. G. Skene, Survey of Recent Advances in Molecular Fluorophores, Unconjugated

Polymers, and Emerging Functional Materials Designed for Electrofluorochromic Use, *Molecules*, 2023, **28**, 3225.
5 K. Nakamura, K. Kanazawa and N. Kobayashi, Electrochemical photoluminescence modulation of functional materials and their electrochemical devices, *J. Photochem. Photobiol., C*, 2022, **50**, 100486.
6 J. Sun, Y. Chen and Z. Liang, Electroluminochromic Materials and Devices, *Adv. Funct. Mater.*, 2016, **26**, 2783–2799.
7 Y. Zhang, E. B. Berda, X. Jia, Z. Lu, M. Zhu and D. Chao, Electrochromic/Electrofluorochromic Supercapacitor Based on a Network Polysiloxane Bearing Oligoaniline and Cyanophenethylene Groups, *ACS Appl. Polym. Mater.*, 2020, **2**, 3024–3033.
8 H. Al-Kutubi, H. R. Zafarani, L. Rassaei and K. Mathwig, Electrofluorochromic systems: Molecules and materials exhibiting redox-switchable fluorescence, *Eur. Polym. J.*, 2016, **83**, 478–498.
9 A. A. Suleymanov, A. Ruggi, O. M. Planes, A.-S. Chauvin, R. Scopelliti, F. Fadaei Tirani, A. Sienkiewicz, A. Fabrizio, C. Corminboeuf and K. Severin, Highly Substituted Δ3-1,2,3-Triazolines: Solid-State Emitters with Electrofluorochromic Behavior, *Chem. - Eur. J.*, 2019, **25**, 6718–6721.
10 Y. Zhuang, S. Guo, Y. Deng, S. Liu and Q. Zhao, Electroluminochromic Materials and Devices Based on Metal Complexes, *Chem. – Asian J.*, 2019, **14**, 3791–3802.
11 J. Luo, Z. Xie, J. W. Y. Lam, L. Cheng, H. Chen, C. Qiu, H. S. Kwok, X. Zhan, Y. Liu, D. Zhu and B. Z. Tang, Aggregation-induced emission of 1-methyl-1,2,3,4,5-pentaphenylsilole, *Chem. Commun.*, 2001, 1740–1741, DOI: 10.1039/B105159H.
12 J. Zhang, H. Zhang, J. W. Y. Lam and B. Z. Tang, Restriction of Intramolecular Motion(RIM): Investigating AIE Mechanism from Experimental and Theoretical Studies, *Chem. Res. Chin. Univ.*, 2021, **37**, 1–15.
13 H. Zhou, M. H. Chua, B. Z. Tang and J. Xu, Aggregation-induced emission (AIE)-active polymers for explosive detection, *Polym. Chem.*, 2019, **10**, 3822–3840.
14 D. Chen, C. Bao, L. Zhang, Q. Zhang, Z. Wu, Z.-Y. Li, X.-Q. Sun, L. Wang and T. Xiao, Dynamic Time-Dependent Emission in Solution and Stable Dual Emission in Solid Matrix Exhibited by a Single-Component Fluorescence System, *Adv. Funct. Mater.*, 2024, **34**, 2314093.
15 T. Xiao, C. Bao, L. Zhang, K. Diao, D. Ren, C. Wei, Z.-Y. Li and X.-Q. Sun, An artificial light-harvesting system based on the ESIPT–AIE–FRET triple fluorescence mechanism, *J. Mater. Chem. A*, 2022, **10**, 8528–8534.
16 Q. Zhang, X. Dang, F. Cui and T. Xiao, Supramolecular light-harvesting systems utilizing tetraphenylethylene chromophores as antennas, *Chem. Commun.*, 2024, **60**, 10064–10079.
17 M. Yu, R. Huang, J. Guo, Z. Zhao and B. Z. Tang, Promising applications of aggregation-induced emission luminogens in organic optoelectronic devices, *PhotoniX*, 2020, **1**, 11.
18 S.-W. Cheng, T. Han, T.-Y. Huang, B.-Z. Tang and G.-S. Liou, High-performance electrofluorochromic devices based on aromatic polyamides with AIE-active tetraphenylethene and electro-active triphenylamine moieties, *Polym. Chem.*, 2018, **9**, 4364–4373.
19 N. Sun, K. Su, Z. Zhou, X. Tian, D. Wang, N. Vilbrandt, A. Fery, F. Lissel, X. Zhao and C. Chen, Synergistic effect between electroactive tetraphenyl-p-phenylenediamine and AIE-active tetraphenylethylene for highly integrated electrochromic/electrofluorochromic performances, *J. Mater. Chem. C*, 2019, **7**, 9308–9315.
20 N. Sun, K. Su, Z. Zhou, D. Wang, A. Fery, F. Lissel, X. Zhao and C. Chen, "Colorless-to-Black" Electrochromic and AIE-Active Polyamides: An Effective Strategy for the Highest-Contrast Electrofluorochromism, *Macromolecules*, 2020, **53**, 10117–10127.
21 N. Sun, K. Su, Z. Zhou, Y. Yu, X. Tian, D. Wang, X. Zhao, H. Zhou and C. Chen, AIE-Active Polyamide Containing Diphenylamine-TPE Moiety with Superior Electrofluorochromic Performance, *ACS Appl. Mater. Interfaces*, 2018, **10**, 16105–16112.
22 H.-J. Yen and G.-S. Liou, Flexible electrofluorochromic devices with the highest contrast ratio based on aggregation-enhanced emission (AEE)-active cyanotriphenylamine-based polymers, *Chem. Commun.*, 2013, **49**, 9797–9799.
23 H.-J. Yen, C.-W. Chang, H. Q. Wong and G.-S. Liou, Cyanotriphenylamine-based polyimidothioethers as multifunctional materials for ambipolar electrochromic and electrofluorochromic devices, and fluorescent electrospun fibers, *Polym. Chem.*, 2018, **9**, 1693–1700.
24 T. Yu, H. Yao, H. Liu and S. Guan, High-performance fluorescent/electroactive (A4 + B2)-type hyperbranched polyimide with AIE-enhanced electroflourochromic behavior, *Dyes Pigm.*, 2023, **214**, 111207.
25 M. H. Chua, K. L. O. Chin, S. J. Ang, X. Y. D. Soo, Z. M. Png, Q. Zhu and J. Xu, Aggregation Induced Emission (AIE)-Active Poly(acrylates) for Electrofluorochromic Detection of Nitroaromatic Compounds, *ChemPhotoChem*, 2022, **6**, e202200168.
26 K. L. O. Chin, P. J. Ong, Q. Zhu, J. Xu and M. H. Chua, Electrofluorochromic Switching of Heat-Induced Cross-Linkable Multi-Styryl-Terminated Triphenylamine and Tetraphenylethylene Derivatives, *Molecules*, 2024, **29**, 2340.
27 S. Mi, J. Wu, J. Liu, Z. Xu, X. Wu, G. Luo, J. Zheng and C. Xu, AIEE-Active and Electrochromic Bifunctional Polymer and a Device Composed thereof Synchronously Achieve Electrochemical Fluorescence Switching and Electrochromic Switching, *ACS Appl. Mater. Interfaces*, 2015, **7**, 27511–27517.
28 Q. Lu, C. Yang, X. Qiao, X. Zhang, W. Cai, Y. Chen, Y. Wang, W. Zhang, X. Lin, H. Niu and W. Wang, Multifunctional AIE-active polymers containing TPA-TPE moiety for electrochromic, electrofluorochromic and photodetector, *Dyes Pigm.*, 2019, **166**, 340–349.
29 S. Yang, Y. Lin, J. Sun, C. Li, Y. Zhang and C. Zhang, Integrated electrochromic and electrofluorochromic properties from polyaniline-like polymers with triphenylacrylonitrile as side groups, *Electrochim. Acta*, 2022, **421**, 140443.
30 S. Hafed-Khatiri, A. F. Quintero-Jaime, D. Salinas-Torres and F. Montilla, Electrofluorochromism of Conjugated Polymers Applied to the Development of Chemical Sensors, *ACS Appl. Electron. Mater.*, 2024, **6**, 847–852.
31 Q. Sun, H. Wang, C. Yang and Y. Li, Synthesis and electroluminescence of novel copolymers containing crown ether spacers, *J. Mater. Chem.*, 2003, **13**, 800–806.

32 M. P. Aldred, C. Li, G.-F. Zhang, W.-L. Gong, A. D. Q. Li, Y. Dai, D. Ma and M.-Q. Zhu, Fluorescence quenching and enhancement of vitrifiable oligofluorenes end-capped with tetraphenylethene, *J. Mater. Chem.*, 2012, **22**, 7515–7528.
33 A. D. Becke, Density-functional thermochemistry. III. The role of exact exchange, *J. Chem. Phys.*, 1993, **98**, 5648–5652.
34 G. Scalmani, M. J. Frisch, B. Mennucci, J. Tomasi, R. Cammi and V. Barone, Geometries and properties of excited states in the gas phase and in solution: theory and application of a time-dependent density functional theory polarizable continuum model, *J. Chem. Phys.*, 2006, **124**, 94107.
35 M. J. Frisch, G. W. Trucks, H. B. Schlegel, G. E. Scuseria, M. A. Robb, J. R. Cheeseman, G. Scalmani, V. Barone, G. A. Petersson, H. Nakatsuji, X. Li, M. Caricato, A. V. Marenich, J. Bloino, B. G. Janesko, R. Gomperts, B. Mennucci, H. P. Hratchian, J. V. Ortiz, A. F. Izmaylov, J. L. Sonnenberg, D. Williams-Young, F. Ding, F. Lipparini, F. Egidi, J. Goings, B. Peng, A. Petrone, T. Henderson, D. Ranasinghe, V. G. Zakrzewski, J. Gao, N. Rega, G. Zheng, W. Liang, M. Hada, M. Ehara, K. Toyota, R. Fukuda, J. Hasegawa, M. Ishida, T. Nakajima, Y. Honda, O. Kitao, H. Nakai, T. Vreven, K. Throssell, J. A. Montgomery, Jr., J. E. Peralta, F. Ogliaro, M. J. Bearpark, J. J. Heyd, E. N. Brothers, K. N. Kudin, V. N. Staroverov, T. A. Keith, R. Kobayashi, J. Normand, K. Raghavachari, A. P. Rendell, J. C. Burant, S. S. Iyengar, J. Tomasi, M. Cossi, J. M. Millam, M. Klene, C. Adamo, R. Cammi, J. W. Ochterski, R. L. Martin, K. Morokuma, O. Farkas, J. B. Foresman and D. J. Fox, *Gaussian 16, Revision C.01*, Gaussian Inc., Wallingford CT, 2016.
36 J.-D. Chai and M. Head-Gordon, Long-range corrected hybrid density functionals with damped atom–atom dispersion corrections, *Phys. Chem. Chem. Phys.*, 2008, **10**, 6615–6620.
37 F. Weigend and R. Ahlrichs, Balanced basis sets of split valence, triple zeta valence and quadruple zeta valence quality for H to Rn: Design and assessment of accuracy, *Phys. Chem. Chem. Phys.*, 2005, **7**, 3297–3305.
38 M. Winslow, W. B. Cross and D. Robinson, Comparison of Spin-Flip TDDFT-Based Conical Intersection Approaches with XMS-CASPT2, *J. Chem. Theory Comput.*, 2020, **16**, 3253–3263.
39 M. Kuss-Petermann and O. S. Wenger, Electron Transfer Rate Maxima at Large Donor–Acceptor Distances, *J. Am. Chem. Soc.*, 2016, **138**, 1349–1358.

